Elastic displacements and step interactions on metallic surfaces: Grazing-incidence x-ray diffraction and *ab initio* study of Au(332)

G. Prévot,[1] Y. Girard,[2] V. Repain,[2] S. Rousset,[2] A. Coati,[3] Y. Garreau,[2,3] Jaita Paul,[4] Nisha Mammen,[4] and Shobhana Narasimhan[4]

[1]*Institut des NanoSciences de Paris, UMR CNRS 7588, Université Pierre et Marie Curie-Paris 6, 140 Rue de Lourmel, 75015 Paris, France*

[2]*Laboratoire Matériaux et Phénomènes Quantiques, UMR CNRS 7162, Université Paris Diderot-Paris 7, Bât. Condorcet, 75205 Paris Cedex 13, France*

[3]*Synchrotron SOLEIL–l'Orme des Merisiers, Saint Aubin, BP 48, 91192 Gif-sur-Yvette Cedex, France*

[4]*Theoretical Sciences Unit, Jawaharlal Nehru Centre for Advanced Scientific Research, Jakkur, Bangalore 560064, India*

(Received 2 October 2009; revised manuscript received 21 January 2010; published 16 February 2010)

We have studied the energetics, relaxation, and interactions of steps on the Au(332) vicinal surface using a combination of grazing incidence x-ray diffraction, anisotropic linear elasticity theory, and *ab initio* density-functional theory. We find that the initial force distribution on a bulk-truncated surface, as well as the resulting pattern of atomic relaxations, can be reproduced excellently by a buried dipole elastic model. The close agreement obtained between experimental and calculated x-ray diffraction profiles allows us to precisely determine the value of the elastic dipole density at the steps. We also use these results to obtain an experimental estimate of the surface stress on an unreconstructed Au(111) facet, $\tau_{\mathrm{Au}(111)}=2.3\pm0.4$ Nm^{-1}, and the value of the step-step elastic interaction energy $A=950\pm150$ meV Å.

DOI: 10.1103/PhysRevB.81.075415 PACS number(s): 68.35.B−, 68.35.Md

I. INTRODUCTION

Vicinal surfaces are obtained by cutting a crystal close to a dense plane. They are characterized by terraces of the dense plane orientation separated by steps. The presence of these steps can be exploited for possible technological applications, e.g., the steps can serve as nucleation centers for the growth of metallic nanowires.[1,2] In such cases, the regularity of the wire organization obtained is determined by the regularity of the array of steps of the bare surface. At finite temperature, steps fluctuate due to thermal motion.[3] The step fluctuations are governed by both the step-step interactions and the kink creation energy. While the kink creation energy is a very local energetic parameter, step interactions have a long-range component.

Different contributions to the step interactions can be distinguished. Steps entropically repel one another through the condition that two steps cannot cross each other; when the steps are close together, the number of allowed configurations is reduced and this reduction of entropy is equivalent to an interstep repulsion.[4] Steps also interact electronically through the modification of the density of states,[5,6] electrostatically due to the presence of electrostatic dipoles at the steps,[7,8] and thermally through the modification of their vibrational free energy.[9] They also interact elastically through the long-range displacement fields generated by atomic relaxations at the steps.[10] It is generally assumed that the most important contribution, at least for large terraces, is the elastic contribution.

Over the years, several authors have come up with elastic models to describe step-step interactions.[10–14] In general, these works assume a model for the force distribution that arises at step edges when a crystal is cleaved to create a vicinal surface; the resulting pattern of displacements and the corresponding elastic energy (and, thus, the elastic step interaction energy) are then obtained using continuum elasticity theory. In recent years, it has become possible to test the validity of these models in two ways: (i) experimentally, by comparison to the results obtained from grazing incidence x-ray diffraction (GIXD), and (ii) computationally, by comparison to the results obtained from *ab initio* density-functional theory (DFT) calculations.

GIXD experiments have been recently performed on vicinal surfaces of transition metals.[15,16] The model of a buried elastic dipole has been shown to well reproduce the experiments and linear elasticity has been used for measuring the elastic interactions between steps on Pt(779) and Cu(223) vicinal surfaces. For both cases, elastic interactions were found to be much higher than electrostatic interactions known from the literature. However, the values found also differed from the values of the step interaction derived from scanning tunneling microscopy (STM) measurements. For Cu(223), the elastic interaction obtained by GIXD was 1 order of magnitude higher than the interaction derived from STM measurements.[17] For Pt(997), it was smaller.[3,18]

There have also been earlier calculations of step energetics using *ab initio* DFT.[19–22] In these calculations, the focus was primarily on obtaining the difference between the formation energies of terraces with the two kinds of close-packed steps possible on a face-centered-cubic (fcc) (111) or hexagonally close-packed (0001) surface. These papers showed that a precise computation of this very small (~10–100 meV/Å) energy difference required extremely precise Brillouin-zone sampling and large unit cells and was therefore computationally demanding. For these reasons, it is very difficult to quantitatively derive the step interaction energy from the angular dependence of the surface energy and only a few *ab initio* results have been obtained concerning the step interaction energy.[23,24]

In this paper, we use both of these approaches for the particular case of the Au(332) surface and show that the re-

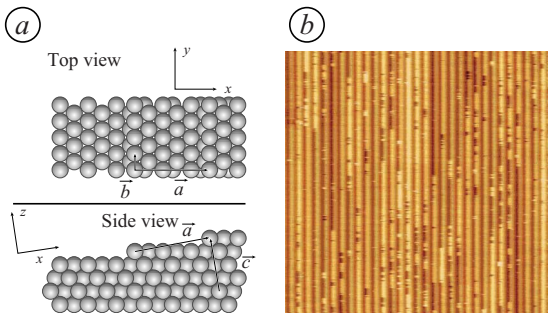

FIG. 1. (Color online) (a) Schematic diagram of the atomic arrangement on the Au(332) surface, including the unit cell $(\vec{a},\vec{b},\vec{c})$ for GIXD measurements and (b) 40 nm STM image of the Au(332) surface.

sults thus obtained correlate well with the buried dipole model introduced by Prévot and Croset.[13,14] In Sec. II, the experimental measurements and theoretical methods are described. The experimental and theoretical results are presented in Sec. III. Section IV is devoted to a precise analysis of the results in the frame of the buried dipole model. We show that a quantitative value of the step interaction energy can be derived from the measurements or from the calculation of the atomic displacements. The conclusions are given in Sec. V.

II. MEASUREMENTS AND CALCULATIONS

A. Sample

The sample was a single crystal consisting of a 4 mm diameter disk, polished to a mirrorlike surface and cut normal to the [332] direction. The fcc (332) surface obtained consists of (111) terraces that are six atomic rows wide, separated by $(11\bar{1})$-faceted steps; a schematic atomistic model is shown in Fig. 1(a). The sample surface is cleaned in ultrahigh vacuum (UHV) by standard Ar ion sputtering at 600 eV for 15 min, followed by annealing at 800 K for 10 min. After ten of these cycles, the crystalline quality of the surface was found to be very good, as checked by the low-energy electron-diffraction (LEED) pattern and STM images over the whole sample. Figure 1(b) shows a typical STM image recorded slightly above room temperature, showing the regular array of step edges and thermal kinks.

B. GIXD

GIXD experiments were performed on the DW12 beamline at LURE-DCI storage ring. The sample was introduced in UHV chambers and the data were collected by means of a z-axis diffractometer. The base pressure in the chambers was 10^{-10} Torr. The sample could be transferred from the analysis chamber to a preparation chamber equipped with a four grid LEED and a cylindrical mirror analyzer Auger spectrometer. The x-ray data collection was performed using 15 keV photons with an incidence angle kept fixed at 0.3°, which corresponds to the angle of total external reflection. To define the basis, we have used the orthogonal vectors

$$\vec{a}=\begin{pmatrix}-1\\-1\\3\end{pmatrix},\quad \vec{b}=\frac{1}{2}\begin{pmatrix}1\\-1\\0\end{pmatrix},\quad \text{and}\quad \vec{c}=\begin{pmatrix}3\\3\\2\end{pmatrix}$$

Therefore, $\vec{a}$ is normal to the steps, corresponding to the distance between two consecutive step edges, which is 13.5 Å, $\vec{b}$ is parallel to the steps, corresponding to the system zone axis (its modulus being the interatomic distance of pure gold, i.e., 2.88 Å), and $\vec{c}$ is normal to the surface plane. In the following, all the data are presented relative to this basis.

The corresponding h, k, and l indices are used for indexing a reflection in reciprocal space. The reciprocal-space transformation from the surface coordinate (hkl) to the standard fcc coordinates (HKL) is given by

$$\begin{bmatrix}H\\K\\L\end{bmatrix}=\frac{1}{22}\begin{bmatrix}-2 & 22 & 3\\-2 & -22 & 3\\6 & 0 & 2\end{bmatrix}\begin{bmatrix}h\\k\\l\end{bmatrix}. \quad (1)$$

We have performed standard rocking scans along various crystal truncation rods (CTRs) for determining the structure factors in different regions of the reciprocal space. The integrated intensities were corrected using the procedure reported in Ref. 25.

C. *Ab initio* calculations

The *ab initio* DFT calculations were performed using the PWSCF code, which forms a part of the QUANTUM-ESPRESSO distribution.[26] The interaction between ions and valence electrons was described using an ultrasoft pseudopotential and exchange-correlation effects were described using the local-density approximation, as parametrized by Perdew and Zunger.[27] A plane-wave basis set was used, with an energy cutoff of 40 Ry for wave functions and 320 Ry for charge densities. We verified that force distributions, atomic displacements, surface energy, and step energy are well-converged with this choice of basis set. However, for computational reasons, it was found that to obtain a well-converged value of the surface stress, it was needed to go to much higher cutoffs of 70 and 560 Ry for wave functions and charge densities, respectively. Brillouin-zone sampling was performed using Monkhorst-Pack meshes, together with the Methfessel-Paxton smearing scheme[28] with a smearing width of 0.05 Ry.

For bulk Au in the fcc structure, we have obtained the lattice parameter as 4.05 Å, which agrees well with the experimental value of 4.08 Å. We have also computed the elastic constants of Au: since one of our aims is to analyze our *ab initio* results within the framework of linear elasticity theory, it is important to correctly reproduce the elastic properties of Au by *ab initio* calculations. For a cubic crystal, there are three independent elastic constants C_{11}, C_{12}, and C_{44}. They were obtained in a standard way:[29] by subjecting a bulk Au fcc crystal to a homogeneous strain, an orthorhombic strain, and a monoclinic strain and then relating the change in total energy to the strain applied.

From this procedure, we have obtained $C_{11}=209.6$ GPa, $C_{12}=182.0$ GPa, and $C_{44}=36.5$ GPa. The corresponding experimental values are 192.4, 163.0, and 42.0 GPa respectively;[30] the agreement between calculated and experimental values is thus found to be reasonable.

We have also tested our *ab initio* calculations on a flat and unreconstructed Au(111) surface. We obtain a surface energy of 0.071 eV/Å^2=1.13 Nm^{-1} and a surface stress of 0.191 eV/Å^2=3.06 Nm^{-1}; these numbers are in reasonably good agreement with previous calculations.[31] We obtain a pattern of near-surface relaxations where the first interlayer distance d_{12} is expanded by 0.78% and the second interlayer spacing d_{23} is contracted by −0.43%, with respect to the bulk interlayer spacing. It is somewhat surprising that d_{12} is expanded since the general expectation is that metal surfaces should relax inward. However, a number of calculations, using both all-electron and pseudopotential methods, have reported an outward expansion of the surface layer on unreconstructed Au(111).[31,32] We note that it is not possible to compare this finding directly to experimental results since the Au(111) surface is actually reconstructed and it is expected that this reconstruction will affect interlayer spacings near the surface.

The calculations on the Au(332) surface were performed using a 17-layer vicinal slab, where the middle layer was kept fixed and the outer layers on both sides were allowed to relax. The force convergence threshold was fixed at 10^{-3} Ry/bohr=0.041 nN. Periodic images were separated by a vacuum of ~14 Å along the z (surface-normal) direction; this corresponds to about six interlayer spacings. The k points used were obtained using a $(3\times12\times1)$ Monkhorst-Pack mesh. It was verified that the displacements away from bulk-truncated positions did not change noticeably on increasing the number of layers in the slab, the vacuum spacing, or number of k points.

Forces were calculated using the Hellmann-Feynman theorem.[33,34] Moreover, we have computed the step formation energy from an appropriate combination of the computed total energies for four different systems: (1) a slab with (332) surfaces on both sides and containing N_1 atoms, (2) a slab with (111) surfaces on both sides and containing N_2 atoms, (3) a single-atom bulk unit cell with k-point sampling commensurate to that used in (1), and (4) a single-unit bulk unit cell with k-point sampling commensurate to that used in (2). The corresponding total energies are denoted as E_1, E_2, E_3, and E_4, respectively. The step formation energy β is then given by

$$\beta = \frac{1}{2}(E_1 - N_1E_3) - \left(\frac{16}{3}\right)\left(\frac{1}{2}\right)(E_2 - N_2E_4). \qquad (2)$$

Here, the factors of $\frac{1}{2}$ appear because the slabs have two surfaces and the factor of $\frac{16}{3}$ is related to the exposed surface area on a vicinal surface that consists of six-row terraces separated by {111}-faceted steps. The reason for the two different values used for bulk energies (E_2 and E_4) is that one hopes, in this way, to obtain a cancellation in the errors due to finite Brillouin-zone sampling. In our case, $N_1=45$ and $N_2=9$.

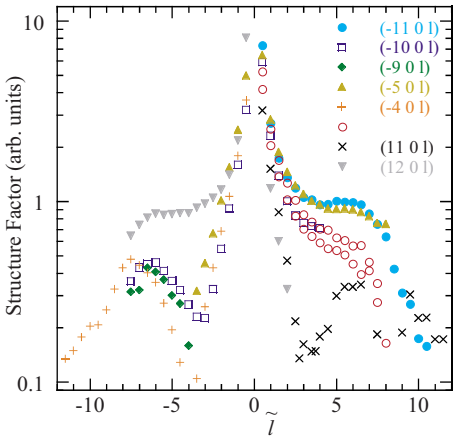

FIG. 2. (Color online) Experimental structure factors of crystal truncation rods on Au(332) as a function of $\tilde{l}=l-l_{\mathrm{Bragg}}$.

III. RESULTS

A. Experimental GIXD results

Along each CTR, the diffracted amplitude is of course maximum at the Bragg position, i.e., at $l=l_{\mathrm{Bragg}}$. However, when going away from the Bragg peak, the amplitude does not decrease smoothly: at particular values of l, sharp variations of the amplitude occur. In Fig. 2, all data points are presented as a function of the momentum transfer $\tilde{l}$ along l with respect to the value corresponding to the nearest Bragg spot: $\tilde{l}=l-l_{\mathrm{Bragg}}$. As can be seen, the positions where the sharp variations occur are often the same for all rods and thus depend mainly on $\tilde{l}$. For example, sharp variations of the amplitude are always present near $\tilde{l}=\pm8$. As has been pointed out previously,[36] these sharp variations are related to elastic displacements penetrating deeply into the bulk; they will be discussed in detail in Sec. IV.

B. *Ab initio* results

As expected, a bulk-truncated Au(332) surface, where all atoms are fixed at the positions they would have in an infinite bulk crystal, is not at equilibrium. The forces on such a bulk-truncated Au(332) slab are presented in Fig. 3(a). Significant forces are experienced primarily by the two atoms at the top

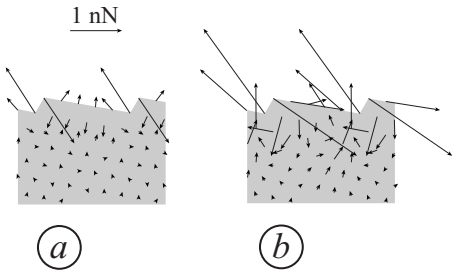

FIG. 3. Results, obtained from *ab initio* density-functional theory calculations, for (a) the force distribution on a bulk-truncated slab with (332) faces and (b) the atomic relaxations, i.e., the displacements away from bulk-truncated positions. For clarity, the relaxations have been amplified by a factor of 50.

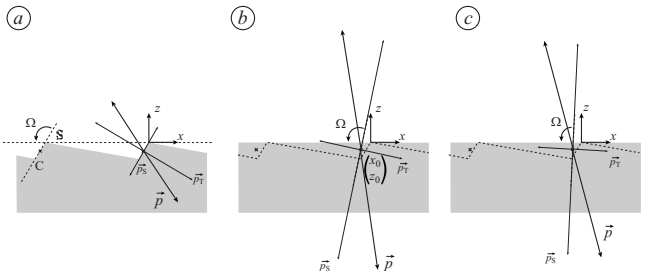

FIG. 4. Schematic diagrams showing the dipolar distributions given in Table I. (a) Point dipole equivalent to the initial force distribution on the step edge (s) and corner (c) atoms computed by DFT for a bulk-truncated slab. (b) Elastic point dipole giving the same displacements as the atomic relaxations computed by DFT. (c) Elastic point dipole that gives the best fit to the GIXD results. Ω is the orientation of the lever arm of the dipole with respect to the surface and x_0 and z_0 are the positions of the dipole with respect to the step edge. The dipole is the sum of a torque component $\vec{p}_T$ and a stretch component $\vec{p}_S$. Note that the (b) and (c) distributions are very similar.

and the bottom of a step edge; the forces on all other atoms are considerably smaller. Moreover, the forces on these two atoms are approximately equal in magnitude ($\sim$1.1 nN/atom) and opposite in direction, with the forces acting in such a way as to favor a rounding of the sharp step edge. Thus, if we were to consider the forces exerted on all the top and bottom corner atoms at a step edge, these are roughly equivalent to a line of force dipoles, with a torque component density of p_T=0.80 nN and a stretch component density p_S=0.41 nN. Such an arrangement of dipoles, obtained by considering only the forces on the atoms directly at the step edge, is depicted in Fig. 4(a). Upon extending this further by taking into account the forces on the seven atoms nearest to the step edge, we obtain p_T=0.90 nN and p_S =0.05 nN. The large change of p_S when extending the calculation to all the atoms is due to the presence of a stretch dipole surface density below the terraces, as can be seen in Fig. 3(a).

In response to this force distribution, atomic positions relax away from their bulk-truncated positions. The resulting pattern of displacements is shown in Fig. 3(b). Not surprisingly, the largest displacements occur for the atoms directly at the top and bottom of the step edge, which move in roughly opposite directions, by about 0.3 Å, resulting in a blunting of the sharp step edge. However, there are appreciable displacements of several other atoms in the vicinity of the step edge; the vectorial pattern of these displacements resembles a vortex. The mean relaxation of the terrace, i.e., the relaxation dz_1' of the six terrace atoms in the (111) direction, is dz_1'=0.041 Å and for the next six atoms, i.e., for the atoms just below the surface, dz_2'=−0.002 Å. The interlayer distance $z_1'-z_2'$ between the terrace plane and the (111) plane below is thus expanded by 2.0% with respect to its bulk value. This relaxation is in the same direction as (but 2.6 times higher than) the relaxation of the first interplanar distance on an unreconstructed Au(111) surface (see Sec. II C).

C. Comparison between experimental and theoretical structure factors

We have used the atomic positions calculated *ab initio* for computing theoretical structure factors. For this purpose, only half of the slab is of course used (from the surface to the middle of the slab used in the simulations). The result of the comparison is drawn in Fig. 5. For this comparison, only two adjustable parameters are introduced: a scale factor and a roughness factor. Vicinal surfaces often exhibit nonnegligible roughness due to the fluctuation of the interstep distance. In GIXD measurements, this causes a broadening of the CTRs when going away from Bragg spots, leading to a loss of intensity when integrating the rocking-scan profiles for obtaining the structure factors. We account for the roughness by making use of the model suggested by Robinson.[35] In this model, the diffracted intensity is corrected by a factor $F_{\text{rough}}=\frac{(1-\xi)^2}{\{1+\xi^2-2\xi\cos[2\pi(l-l_0)/\Delta l]\}}$, where l_0 is the position of a Bragg spot along the rod and Δl is the distance between two consecutive Bragg spots along a rod. In our case, Δl=44. In the model of Robinson, the roughness exponent, ξ, is related to the fractional occupancy of the planes above the reference surface. More precisely, ξ^n is the probability of finding an atom in the nth plane above the surface. ξ=0 for an ideal surface and ξ=1 for a surface above the roughening transition. In our case, the planes that have to be considered are the (332) planes. Thus, for vicinal surfaces, small variations of the terrace width lead to a strong increase in the value of ξ.

F_{rough} varies slowly with l. Without taking roughness into account, the theoretical structure factors measured far from the Bragg spots are on average always higher than the experimental ones. The variations of the amplitude of the diffracted wave are qualitatively well reproduced by the theory with a roughness exponent ξ=0.38. Note that in our case, the maximum value of $|l-l_0|/\Delta l$ is 0.27, giving rise to a maximum attenuation of the diffracted intensity by a factor F_{rough}=0.31.

As can be seen in Fig. 5, the positions of the minima of amplitude along the rods are well reproduced by the simulation. However, considering the logarithmic scale in the intensity, some rods are not perfectly fitted and require a more refined analysis. This is the case, for example, for the $(\bar{1}00l)$ and $(\bar{1}10l)$ rods. This indicates that the *ab initio* results, although rather close to the experiments, are not perfectly in agreement with them.

Note that modifying the theoretical values of displacement by introducing a simple scale factor does not lead to a significant improvement in the quality of the fit. Determining the individual atomic displacements independently is also not practicable because of the very large number of variables involved. We have to find another approach toward fitting the experimental results. Moreover, it is still desirable to understand the underlying physics that governs the pattern of relaxations and to estimate the importance of the different factors governing the step interactions. With such a goal in mind, in the following, we perform an analysis of the database on linear elasticity theory, with adjustable parameters for the dipole of forces at the step edge, in order to obtain a precise value of the step-step interaction. Indeed, we will show by comparison to the *ab initio* results that the buried

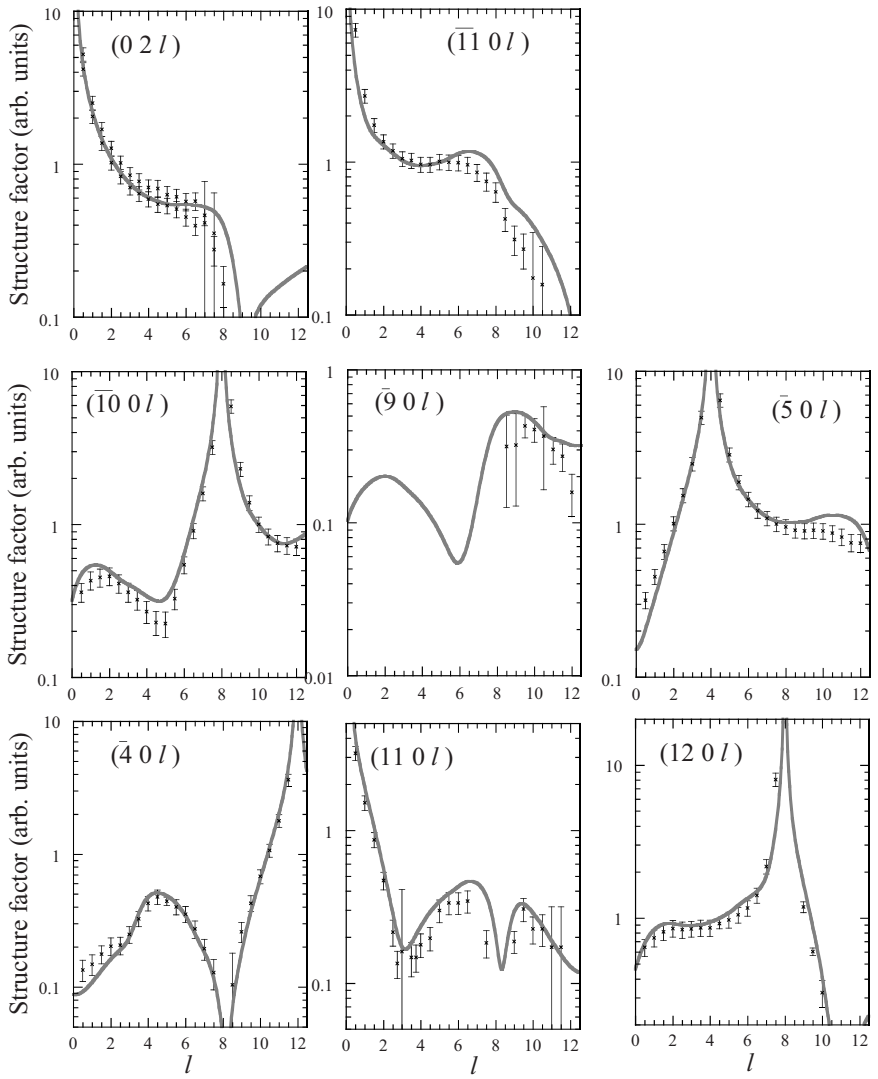

FIG. 5. Comparison between experimental and theoretical structure factors for Au(332). Dots are the experimental data, while lines are the values calculated making use of the *ab initio* DFT results for atomic relaxations.

dipole model gives, with a very high accuracy, the atomic displacements, even for atoms very close to the step edge.

IV. RESULT ANALYSIS

A. Origin of the modulation of the amplitude along the rods

For a vicinal surface, the variations of the diffracted amplitude have been ascribed to the elastic relaxation modes near the surface of the crystal.[36] Atomic relaxations for atoms near the step occur due to the change in the number and symmetry of neighboring atoms and the modification of the local electronic density of states near the steps. These relaxations propagate elastically into the bulk. Since the steps form a periodic array of straight lines at the surface of the crystal, the elastic displacements are expressed naturally as a Fourier series where each mode takes the form

$$\vec{u} = \sum_{q_z} \vec{u}_0(q_z)\exp(iq_z z)\exp(iq_x x), \tag{3}$$

where $\vec{u}$ is the elastic displacement, q_x is the wave vector in the direction parallel to the surface and perpendicular to the step, and q_z is a complex number. Since the steps are periodically spaced, with an interstep distance d, we have $q_x = 2\pi p/d$, where p is an integer. These elastic modes have been studied by Croset and Prévot,[13,14] who showed that for each value of q_x, there exist only three possible elastic modes with $q_z = kq_x$; here, k is a complex number with negative imaginary part, resulting from the resolution of a sixth-order secular equation. k depends only on the elastic constants of the crystal and on the direction of q_x.[13] Moreover, in the case where $(x0z)$ is a plane of symmetry, the secular equation reduces to a fourth-order equation and only two modes have to be considered. This is still the case for the $[1\bar{1}0]$ steps running on the (332) surface of a cubic crystal. For Au(332), the resolution of the fourth-order equation for $q_x > 0$ gives the following values for k: $k_1 = -0.88 - 1.47i$ and $k_2 = +0.26 - 0.49i$.[13] The real part of k gives the propagation direction for the elastic modes, whereas the imaginary part gives the attenuation in depth of the displacements and is thus negative since $z < 0$ in the bulk. Note that in the case of an isotropic crystal, one always obtains $\mathrm{Im}(k) = -1$. For Au(332), the first mode is thus more rapidly attenuated, whereas the second

mode penetrates deeper into the bulk. For Au(332), the interstep distance is $d=13.5$ Å. The attenuation length of the second mode is thus $-d/2\pi\,\mathrm{Im}(k_2)=4.4$ Å.

A first-order expansion of the expression for the diffracted amplitude allows us to easily interpret the GIXD results.[36] To each elastic displacement mode correspond new diffraction satellites, apart from the Bragg spot. The position of the satellites with respect to the Bragg spots is given by $\mathrm{Re}(\vec{q})$. Moreover, due to the fact that the spacing between the rods is given by $2\pi/d$, the diffraction satellites are located on crystal truncation rods. The position of these satellites on a rod is given by[36]

$$\tilde{l}=l-l_{\mathrm{Bragg}}=q_x\,\mathrm{cotan}\,\theta-\mathrm{Re}(q_z), \tag{4}$$

where θ is the miscut angle of the vicinal surface. The interference between the amplitudes associated with the diffraction satellites and the fundamental of the rod determines the shape of the sharp variations that are observed on the rods. Note also that the full width at half maximum of the diffraction satellites along l is $-\sqrt{3}\,\mathrm{Im}(q_z)$.

Let us consider the first positive harmonic of the elastic displacements, $q_x=2\pi/d$. For Au(332), using our system of reduced units, q_x cotan $\theta=8$. The satellite associated with the first elastic mode, for which $\mathrm{Re}(q_z)=q_x\,\mathrm{Re}(k_1)=-1.2$, appears thus at $\tilde{l}_1=9.2$ with a width $w_1=3.6$ whereas the satellite associated with the second elastic mode for which $\mathrm{Re}(q_z)=0.4$ appears at $\tilde{l}_2=7.6$ with a narrower width $w_2=1.2$. The relative intensity of the satellite depends mainly on the product $\vec{Q}\vec{u}_0$, where $\vec{Q}$ is the scattering vector and $\vec{u}_0$ is defined in Eq. (3). As a result, since Q_x varies from one rod to another, the different rods do not exhibit the same shape. The measurement of two rods at different positions of the reciprocal space should allow one to separate out the contribution of the two modes for each value of q_x.

B. Elastic relaxations

It should be possible to directly access the elastic relaxation modes by measuring the diffracted amplitude along crystal truncation rods. In the case of elastic displacements due to steps on a vicinal surface, the different elastic modes can also be derived from the distribution of elastic forces equivalent to a step. As already mentioned, steps on vicinal surfaces are equivalent to lines of force dipoles.[10,13] Using Hooke's law and mechanical equilibrium at the surface and in the bulk, it is possible to derive the elastic displacements due to the dipoles. The different harmonics of the force distribution are obtained by a Fourier transform of the force density distribution near the step. While *ab initio* calculations (such as the ones presented in this paper) now enable us to obtain the atomistic force distribution, in order to go over to a continuum description that is free of singularities, one has to use some smoothened form to describe the variation in the forces along x. Generally, a combination of Lorentzian profiles along the x direction is assumed.[13,14] Steps are thus described by opposite lines of forces forming lines of elastic dipoles. When such an approximation is made, analytical formulas can easily be obtained.[13,14]

For a given vicinal surface, the dipole orientation, the position with respect to the step edge, and the lever arm orientation of the dipoles are *a priori* unknown. However, these parameters can be derived from numerical simulations using either *ab initio* calculations or some parametrized model for interatomic interactions. Such a procedure has previously been carried out for vicinal surfaces of transition metals using semi-empirical potentials derived from tight-binding considerations.[37] However, the comparison to experimental results obtained for Pt and Cu vicinals[15,16] showed that the predicted displacements were roughly 2 times lower than the experimental ones.

We have mentioned in Sec. III B above that the force distribution computed by *ab initio* DFT calculations on an unrelaxed bulk-truncated slab is equivalent to a dipolar distribution. We have also checked that the calculated atomic displacements are in good agreement with the response to an elastic dipole. For this purpose, we have compared the atomic relaxations presented in Fig. 3(a) to the result of an elastic calculation with lines of point dipoles at the steps. Five free parameters, namely, the amplitude, orientation, positions with respect to the step edge along x and z, and the lever arm orientation of the dipoles are adjusted in order to obtain the best agreement with the *ab initio* results for relaxation. We find that the calculated relaxations are equivalent to the elastic response of an elastic dipole density having a torque component $p_T=0.61\pm0.04$ nN and a stretch component $p_S=1.8\pm0.3$ nN. The dipole orientation is presented in Fig. 4(b). The value of p_T is close to the value derived from the initial force distribution, whereas the value of p_S is very different. The difference between the value of p_T determined from the initial force distribution and the value of p_T determined from the comparison to linear elasticity could be due to a modification of the elastic constants at the surface and especially near the step edge. A stiffening of some elastic constants has been found near the steps of vicinal surfaces of transition metals.[38] Such effects are not taken into account in our linear elasticity calculations. A stiffening of the elastic constants at the step edge could thus explain the higher value obtained for the dipole directly calculated from the initial force distribution.

However, such effects cannot explain the differences observed for the value of p_S. The high value of p_S determined by linear elasticity calculations could be due to the fact that these calculations also fit the stretch dipoles that are present below the terraces. Moreover, the contribution of stretch dipoles to the atomic displacements is much smaller than torque dipoles[13,37] and a high value of p_S can be compensated by a small reduction of p_T. Thus, p_S is not a very relevant parameter for describing the atomic relaxations. The dipole that gives the best fit to the computed relaxations is located 0.97 Å below the step edge, with a shift of −1.07 Å along the x direction. In Fig. 6, we compare the relaxations calculated analytically using linear elasticity theory (dotted lines) to those obtained by numerical simulation using DFT (filled circles). The close agreement between these two sets of data shows that, at least for Au(332), approximating steps by buried point dipoles works remarkably well. Excepting the relaxations along x of the atoms just below the terrace plane, all relaxations are very well reproduced. This justifies

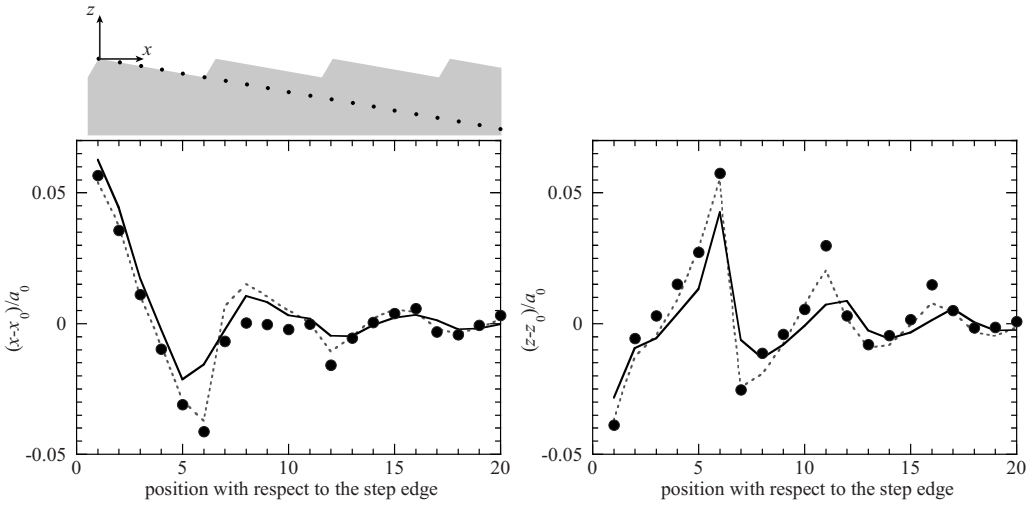

FIG. 6. Atomic relaxations along x and z on Au(332). The atoms are numbered according to their position along a $[\bar{1}\bar{1}2]$ axis, shown in the upper schematic. Filled circles depict relaxations calculated using *ab initio* DFT; dotted lines indicate the elastic response to a point dipole fitted to the *ab initio* relaxations, drawn in Fig. 4(b) and corresponding to the second column of Table I; continuous line shows elastic response to a point dipole fitted to the GIXD results, drawn in Fig. 4(c) and corresponding to the third column of Table I.

the following choice for analyzing our GIXD data: we have fitted the diffracted amplitude with the elastic displacements calculated analytically using the model of lines of buried dipoles. We have used nine free parameters: the positions x_0 and z_0 of the lines of dipoles with respect to the step edge, the width a_c of the Lorentzian shape, the lever arm orientation of the dipoles Ω, the two components of the dipole: the stretch component p_S and the torque component p_T, a roughness factor ξ, and the mean relaxations, dz_1' and dz_2', of the two first terrace planes in the (111) direction.

Using the values indicated in the last column of Table I for these parameters, a perfect fit of the experimental data is obtained. The comparison between measured and simulated amplitudes using an adjustable dipole is shown in Fig. 7. All rods are well reproduced. The values found for dz_1' and dz_2' are small, in accordance with the theoretical predictions. In fact, the quality of the fit depends mainly on the values of two parameters: ξ and p_T. As already mentioned, ξ is given by the surface roughness and determines the overall attenuation of the intensity far from the Bragg spots while p_T determines mainly the amplitude of the sharp variations in diffracted intensity. We thus obtain the same value of ξ as in Sec. III C, namely, ξ=0.38. For p_T, we obtain a slightly lower value than the theoretical one p_T=0.5 nN instead of 0.61 nN.

In Table I, we have also given the corresponding parameters for the elastic dipole equivalent to a step in order to obtain the *ab initio* results for atomic relaxations. The values found for the two sets of parameters (second and third columns in Table I) are very close, which explains why the fit was already good when using directly the values computed by *ab initio* DFT. From the comparison to experiments, it appears however that the theoretical value of p_T is slightly higher than the experimental value. It is possible that the value of p_T experimentally measured is slightly underestimated due to step disorder. As has been pointed out,[36] step disorder reduces the contribution of integer-order harmonics

TABLE I. Parameters describing the elastic dipoles used for fitting the *ab initio* and GIXD results. (x_0, z_0) is the position of the lines of dipoles with respect to the step edge, a_c is the width of the Lorentzian shape, Ω is the lever arm orientation of the dipoles, p_S and p_T are the stretch component and the torque component of the dipole, and dz_1' and dz_2' are the mean relaxations of the two first terrace planes in the [111] direction. For *ab initio* calculations, two sets of values are given. In the left column, indicated are the parameters deduced from the values of the forces exerted on the step edge and corner atoms on a bulk-truncated slab. In this case, x_0 and z_0 are at the midpoints of the step edge and step corner positions and Ω is given by the step orientation. In the second column, given are the values obtained from the comparison to linear elasticity calculations. In the table, also given are the elastic constants used in the linear elasticity calculations and the value of the dipole interaction energy E_2.

	Ab initio		
	Initial forces	Comparison to elasticity	GIXD
Schematic	Figure 4(a)	Figure 4(b)	Figure 4(c)
x_0 (Å)	−0.61	−1.07	−1.02
z_0 (Å)	−1.09	−0.97	−0.94
$\ln(a_c/a_0)$		−3.9	−2.8
Ω (degrees)	119	102	93
p_S (nN)	0.41	1.8 ± 0.3	1.7 ± 0.5
p_T (nN)	0.80	0.61 ± 0.04	0.50 ± 0.08
dz_1' (Å)		0.001	0.016
dz_2' (Å)		0.001	0.016
C_{11} (GPa)		209.6	192.44
C_{12} (GPa)		182.0	162.98
C_{44} (GPa)		36.5	42.00
a_0 (Å)		4.05	4.08
E_2 (meV/at)		860 ± 150	720 ± 180

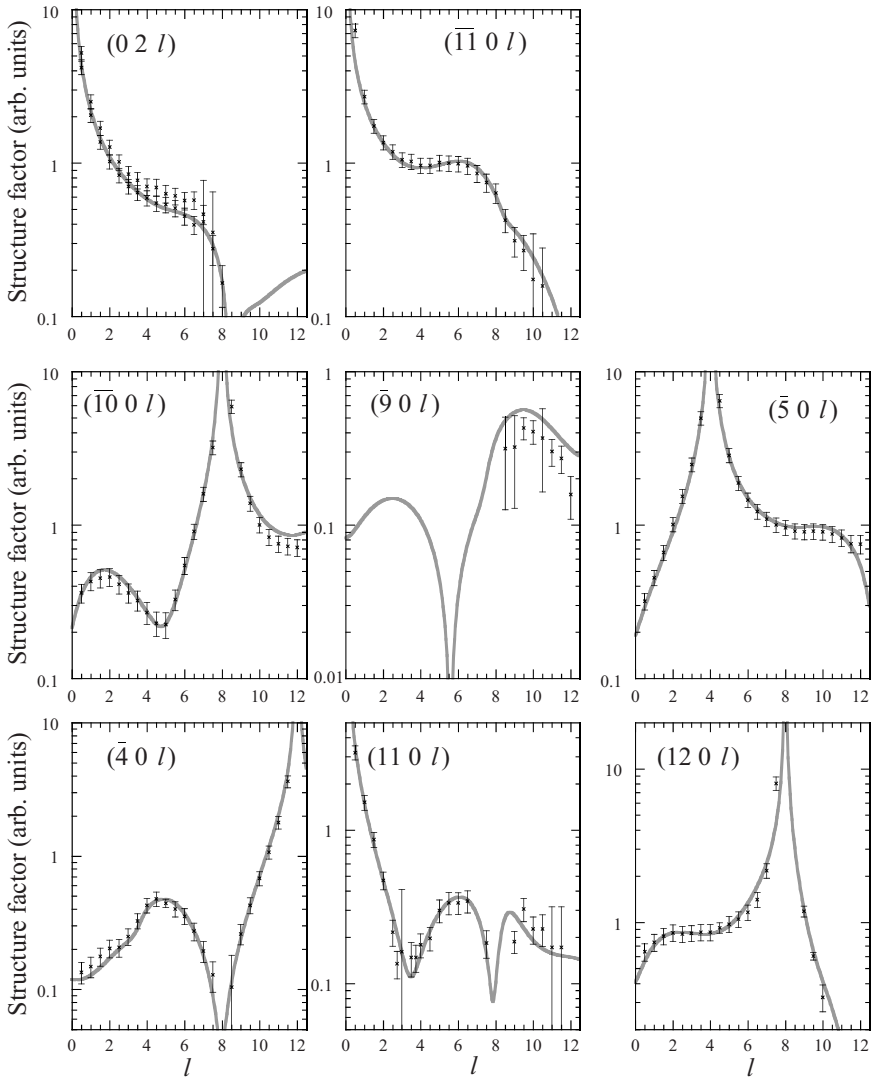

FIG. 7. Comparison between experimental and theoretical structure factors for Au(332). Dots: experiments; full line: simulation with elastic displacements due to lines of dipoles. The parameters used for the elastic displacements are given in the third column of Table I.

in the Fourier decomposition of the elastic displacements. Since only these harmonics contribute to the measured signal, step disorder leads to a decrease of the value of p_T measured, in comparison to data obtained on a perfect surface.

The elastic displacements corresponding to the best fit of the GIXD data with an elastic dipole are drawn in Fig. 6. As already mentioned, these displacements depend mainly on the value of p_T. This is due to the fact that elastic displacements due to pure stretch dipoles are much smaller than displacements due to pure torque dipoles.[13,37] Since GIXD is sensitive to atomic displacements, the uncertainty in the computed value of p_T is thus much smaller than the uncertainty in p_S. The comparison to *ab initio* results shows that the atomic relaxations measured along x are close to the relaxations computed *ab initio*, whereas the atomic relaxations along z are approximately one third lower than the theoretical relaxations.

C. Surface stress

It is very interesting to precisely measure p_T since its value can be directly related to the surface stress of the nominal surface $\tau_{\mathrm{Au}(111)}$,

$$p_T = h_{\mathrm{Step}} \tau_{\mathrm{Au}(111)}, \tag{5}$$

where h_{Step} is the step height. This equation, first stated by Marchenko and Parchin,[10] has been shown to be correct for a lot of vicinal surfaces, in particular for Au(111) vicinals.[37] Inverting Eq. (5), one obtains $\tau_{\mathrm{Au}(111)}=2.1$ Nm^{-1}. Since Au(332) vicinals are not reconstructed, we measure here the surface stress of an unreconstructed Au(111) surface. Such an experimental determination of the surface stress for Au(111) has not, to the best of our knowledge, been performed by other techniques. Some measurements of the mean surface stress τ_{Au} of small crystalline particles have been performed. For example, Solliard and Flueli[39] found $\tau_{\mathrm{Au}}=3$ Nm^{-1}, but the method used does not allow one to

separate the contributions of the different facet orientations. The difference between the surface stress of a reconstructed and an unreconstructed Au(111) surface have also been measured, but measurements have been performed in solution[40] and the absolute value of the surface stress could not be determined from the experiments.

However, several previous authors have performed *ab initio* DFT calculations where they have computed the surface stress on Au(111); they obtained values of $\tau_{\mathrm{Au}(111)}=3.3\ \mathrm{Nm}^{-1}$,[41] $2.6\ \mathrm{Nm}^{-1}$,[42] and $2.8\ \mathrm{Nm}^{-1}$.[43] In this study, we have found a quite similar value, with $\tau_{\mathrm{Au}(111)}=3.06\ \mathrm{Nm}^{-1}$. Using this value and $h_{\mathrm{Step}}=0.236$ nm in Eq. (5), we obtain $p_T=0.72$ nN. This value is slightly lower than the values obtained from our *ab initio* DFT computation of forces (0.8–0.9 nN) and slightly higher than the value of the elastic dipole that fits the *ab initio* DFT calculations (0.61 nN). This indicates that, using this method, a quite good precision on the surface stress value should be obtained.

We point out that the surface stress on an unreconstructed Au(111) facet is a parameter of considerable interest since it has been shown to play a key role in the self-organization of Au(111) vicinal surfaces.[44] It is also important to know its value since it could play a role in the mechanisms leading to the $22\times\sqrt{3}$ reconstruction of Au(111).[32,43] From the comparison between experiments and theory, we can make two hypotheses for determining the surface stress. In the first hypothesis, assuming that Eq. (5) is still valid and using the experimental value $p_T=0.50$ nN, we obtain $\tau_{\mathrm{Au}(111)}=2.1\ \mathrm{Nm}^{-1}$. In the second hypothesis, we notice that the torque component of the elastic dipole density which fits the GIXD results is 18% lower than the one that fits the *ab initio* results and we assume that the same factor should apply for the surface stress. In that case, we obtain $\tau_{\mathrm{Au}(111)}=2.5\ \mathrm{Nm}^{-1}$. These two values differ by only 16%. Thus, from the experimental uncertainty on the value of p_T and from the uncertainty on the derivation of $\tau_{\mathrm{Au}(111)}$ using the elastic dipole density, we estimate that our GIXD determination of the surface stress is $\tau_{\mathrm{Au}(111)}=2.3\pm0.4\ \mathrm{Nm}^{-1}$.

D. Elastic interactions

From the experimentally measured value of the elastic dipoles, the elastic interaction energy between two straight steps can be obtained. The interaction energy β_{int} between two steps is, in a first-order approximation, inversely proportional to the square of the interstep distance:[10] $\beta_{\mathrm{int}}(\theta)=A/d^2+O(1/d^3)$. For a regular array of steps, this interaction sums to the step energy β_0 of an isolated step so that the step energy can be written as

$$\beta=\beta_0+\frac{\pi^2}{6}\frac{A}{d^2}=\beta_0+\frac{E_2}{d^2}. \tag{6}$$

For a regular vicinal surface, A depends only on the value of the elastic dipoles, on the values of the elastic constants, and on the surface orientation.[14] In particular, A depends quadratically on p_S and p_T, with a prefactor depending on the lever arm orientation. Except for Ω close to 0 or π, i.e., when the lever arm of the dipoles is practically parallel to the surface, the contribution of p_S is much smaller than the contribution of p_T. This means that except for this particular lever arm orientation, dipoles that give rise to small elastic displacements also give rise to small interaction between steps. This is still the case here since $\Omega\approx\pi/2$.

Using the values of the elastic dipoles determined by GIXD and equations given in Ref. 14, we find $E_2=720\pm180$ meV/at for d expressed in number of atomic rows. This corresponds to a value $A=950\pm150$ meV Å, when all distances are expressed in Å. The value of elastic step interactions on Au(332) is thus much higher than the value of the elastic step interactions on Cu(223), for which an experimental value of $E_2\approx50$ meV/at has been found,[16] but closer to the value found for step interactions on Pt(779), for which $E_2\approx400$ meV/at.[11] It is also possible to compute elastic interactions from *ab initio* results using the values of the theoretical elastic dipole that fits the computed atomic relaxations. In that case, we find $E_2=860$ meV/at. Since the relaxations calculated *ab initio* are slightly higher than the values found by GIXD, the elastic interactions are also found to be higher.

We can compare the step elastic interaction to the step formation energy computed using Eq. (2), which gives $\beta=248$ meV/at. Using $E_2=860$ meV/at and $d\approx5.4$ rows, we find that $E_2/d^2=29$ meV/at and thus $\beta_0=219$ meV/at. Experimentally, we are not able to measure this quantity since we do not know the nonelastic part of the step formation energy, i.e., the local cost for reducing the number of neighbors for step edge atoms. However, the fact that *ab initio* calculations reproduce quite well atomic relaxations could indicate that the value of β_0 computed is quite good.

V. CONCLUSION

We have measured by GIXD the crystal truncation rods of an Au(332) surface. These data have been analyzed both by a direct comparison to *ab initio* calculations and by a model based on linear elasticity. We have shown that the experimentally obtained diffraction profiles are in good agreement with the displacements obtained from our *ab initio* calculations. Moreover, the calculated atomic displacements can be well reproduced by a simple elastic model with a buried line of dipoles. The comparison between the results obtained by the fit of GIXD experiments and the *ab initio* simulations shows that the main parameter, which is the torque dipole generated by the step edge, is slightly overestimated by *ab initio* calculations, in relation with the calculated surface stress value, for which we are able to obtain the absolute value. The small differences between experiments and simulations could be due to the experimental roughness along the step edges which is not taken into account in the analysis or to fine details of the *ab initio* calculations, for example, related to the fact that the computed values of the elastic constants differ from the experimental values. This provides a good test to check the importance of different terms in the

calculations of atomic displacements by these methods. Finally, the value of the step edge torque dipole allows us to estimate the strength of the step-step interaction on Au(111) vicinal surfaces, which is found to be high as compared to other metallic surfaces. This explains the narrow terrace width distribution observed on these surfaces, which can be a crucial parameter for the measurements of physical properties of naturally nanopatterned surfaces.[45]

ACKNOWLEDGMENTS

We acknowledge financial support from the French Ministry of Research, the CEFIPRA (Indo-French center for the promotion of advanced research, Project No. 3608_2), the ANR (National Research Agency), and the Region Ile-de-france (CNANO and SESAME 2005).

[1] P. Gambardella, Ž. Šljivančanin, B. Hammer, M. Blanc, K. Kuhnke, and K. Kern, Phys. Rev. Lett. **87**, 056103 (2001).
[2] F. J. Himpsel, J. L. McChesney, J. N. Crain, A. Kirakosian, V. Pérez-Dieste, N. L. Abbott, Y.-Y. Luk, P. F. Nealey, and D. Y. Petrovykh, J. Phys. Chem. B **108**, 14484 (2004).
[3] H.-C. Jeong and E. D. Williams, Surf. Sci. Rep. **34**, 171 (1999).
[4] M. E. Fisher and D. S. Fisher, Phys. Rev. B **25**, 3192 (1982).
[5] S. Papadia, M.-C. Desjonquères, and D. Spanjaard, Phys. Rev. B **53**, 4083 (1996).
[6] F. Raouafi, C. Barreteau, M.-C. Desjonquères, and D. Spanjaard, Surf. Sci. **505**, 183 (2002).
[7] R. Smoluchowski, Phys. Rev. **60**, 661 (1941).
[8] L. Peralta, E. Margot, Y. Berthier, and J. Oudar, J. Microsc. Spectrosc. Electron. **3**, 151 (1978).
[9] C. Barreteau, F. Raouafi, M.-C. Desjonquères, and D. Spanjaard, J. Phys.: Condens. Matter **15**, S3171 (2003).
[10] V. I. Marchenko and A. Ya. Parchin, Sov. Phys. JETP **52**, 129 (1980).
[11] L. E. Shilkrot and D. J. Srolovitz, Phys. Rev. B **53**, 11120 (1996).
[12] R. V. Kukta, A. Peralta, and D. Kouris, Phys. Rev. Lett. **88**, 186102 (2002).
[13] G. Prévot and B. Croset, Phys. Rev. Lett. **92**, 256104 (2004).
[14] B. Croset and G. Prévot, Phys. Rev. B **73**, 045434 (2006).
[15] G. Prévot, P. Steadman, and S. Ferrer, Phys. Rev. B **67**, 245409 (2003).
[16] G. Prévot, A. Coati, and Y. Garreau, Phys. Rev. B **70**, 205406 (2004).
[17] M. Giesen and G. Schulze Icking-Konert, Surf. Rev. Lett. **6**, 27 (1999).
[18] T. L. Einstein, H. L. Richards, S. D. Cohen, and O. Pierre-Louis, Surf. Sci. **493**, 460 (2001).
[19] R. Stumpf and M. Scheffler, Phys. Rev. Lett. **72**, 254 (1994).
[20] P. J. Feibelman, Phys. Rev. B **52**, 16845 (1995).
[21] P. J. Feibelman, Phys. Rev. B **60**, 11118 (1999).
[22] P. J. Feibelman, Phys. Rev. B **62**, 17020 (2000).
[23] J. L. F. Da Silva, C. Barreteau, K. Schroeder, and S. Blugel, Phys. Rev. B **73**, 125402 (2006).
[24] D. Yu, H. P. Bonzel, and M. Scheffler, Phys. Rev. B **74**, 115408 (2006).
[25] O. Robach, Y. Garreau, K. Aïd, and M. B. Véron-Jolliot, J. Appl. Crystallogr. **33**, 1006 (2000).
[26] www.quantum-espresso.org
[27] J. P. Perdew and A. Zunger, Phys. Rev. B **23**, 5048 (1981).
[28] M. Methfessel and A. T. Paxton, Phys. Rev. B **40**, 3616 (1989).
[29] M. J. Mehl, J. E. Osburn, D. A. Papaconstantopoulos, and B. M. Klein, Phys. Rev. B **41**, 10311 (1990).
[30] D. R. Lide, *CRC Handbook of Chemistry and Physics*, 75th ed. (CRC Press, Boca Raton, 1995).
[31] N. Takeuchi, C. T. Chan, and K. M. Ho, Phys. Rev. B **43**, 13899 (1991).
[32] V. Zólyomi, L. Vitos, S. K. Kwon, and J. Kollár, J. Phys.: Condens. Matter **21**, 095007 (2009).
[33] H. Hellmann, *Einführung in die Quantenchemie* (Franz Deuticke, Leipzig, 1937).
[34] R. P. Feynman, Phys. Rev. **56**, 340 (1939).
[35] I. K. Robinson, Phys. Rev. B **33**, 3830 (1986).
[36] G. Prévot, B. Croset, A. Coati, and Y. Garreau, J. Appl. Crystallogr. **40**, 874 (2007).
[37] G. Prévot and B. Croset, Phys. Rev. B **74**, 235410 (2006).
[38] A. Kara and T. S. Rahman, Surf. Sci. Rep. **56**, 159 (2005).
[39] C. Solliard and M. Flueli, Surf. Sci. **156**, 487 (1985).
[40] C. E. Bach, M. Giesen, H. Ibach, and T. L. Einstein, Phys. Rev. Lett. **78**, 4225 (1997).
[41] Y. Umeno, C. Elsässer, B. Meyer, P. Gumbsh, M. Nothaker, J. Weissmüller, and F. Evers, Europhys. Lett. **78**, 13001 (2007).
[42] J. Kollar, L. Vitos, J. M. Osorio-Guillen, and R. Ahuja, Phys. Rev. B **68**, 245417 (2003).
[43] R. J. Needs and M. Mansfield, J. Phys.: Condens. Matter **1**, 7555 (1989).
[44] S. Rousset, F. Pourmir, J.-M. Berroir, J. Klein, J. Lecoeur, P. Hecquet, and B. Salanon, Surf. Sci. **422**, 33 (1999).
[45] A. Mugarza, A. Mascaraque, V. Pérez-Dieste, V. Repain, S. Rousset, F. J. García de Abajo, and J. E. Ortega, Phys. Rev. Lett. **87**, 107601 (2001).